An Image-Dependent Metz Filter for Nuclear Medicine Images

Michael A. King, Bill C. Penney, and Stephen J. Glick

Department of Nuclear Medicine, University of Massachusetts Medical Center, Worcester, MA

To provide optimal image quality, digital filters should account for both the count level and the object imaged. That is, they should be image-dependent. By using the constraint equation of constrained least-squares (CLS) restoration to determine one parameter of the Metz filter, a filter which adapts to the image has been developed. This filter has been named the Constrained Least-Squares Metz filter. The filter makes use of a regression relation to convert the Metz filter parameter determined using the CLS criterion to the value which would minimize the normalized mean square error (NMSE). The regression relation and the parameters which specify the general form of the Metz filter were determined using images of the Alderson liver and spleen phantoms. The designed filter was tested for its ability to adapt to other objects with images from each of three different test objects. When the values of the Metz filter parameters for these images determined by the CLS-Metz filter were compared by a regression analysis to those which minimized the NMSE for each image, a correlation coefficient of 0.98, a slope of 0.95, and a zero intercept of 0.1 were obtained. With clinical images, the CLS-Metz filter has been shown to provide consistently good image quality with images as diverse as heart perfusion images and bone studies.

J Nucl Med 29:1980–1989, 1988

During the process of image acquisition, nuclear medicine images are degraded by the limited spatial resolution of cameras and collimators, by scatter and septal penetration, and by Poisson noise which is inherent in the radioactive decay process. The use of two-dimensional restoration has been shown to be able to improve planar image quality (*1–4*). Also, a significant improvement in the quality of single-photon emission computed tomographic (SPECT) images has been demonstrated through the use of two-dimensional pre-reconstruction filtering of SPECT acquisition images (*5–9*).

In the frequency domain, linear restoration filters usually consist of the product of two terms. The first term is the inverse filter, which is the reciprocal of the system modulation transfer function (MTF). This term is used to reduce (or deconvolve) the biases introduced into the image during acquisition. The second term is a low-pass filter, which is used to reduce high-frequency noise. The balance between these two terms is dependent upon the object, the MTF, and the count-level at which the object is imaged. Thus, image-dependent filters (i.e., filters which adapt to the object, the degree of blurring, and the noise content of the image) should be employed for maximal gain in image quality.

The success of the constrained least-squares (CLS) filter in adapting to images of different organ systems (*10,11*) provided motivation for the formulation of an automatically adaptive, image-dependent Metz filter. The CLS filter adapts through the iterative solution of a constraint equation. This constraint equation selects the filter which makes the square of the residual error (difference between the original image and the re-blurred, restored image) equal to the total noise energy (*10–12*). By substituting the Metz filter in place of the CLS filter in the constraint equation, an image-dependent formulation of the Metz filter was obtained which we have called the CLS-Metz filter. When comparing the Metz filters selected using the constraint equation with those selected according to the minimization of the normalized mean square error (NMSE) as previously used with the count-dependent Metz filter (*1,5, 8*), it was noted that the filters were generally significantly different. However, a regression relation was determined to be able to convert the CLS determined filter into the filter selected on the basis of minimization of the NMSE. As a test of the ability of this method to

Received Nov. 10, 1987; revision accepted Jul. 22, 1988.

For reprints contact: Michael A. King, PhD, Dept of Nuclear Medicine, University of Massachusetts Medical Center, 55 Lake Ave. North, Worcester, MA 01655-2397.

adapt to the degraded image, CLS-Metz filters designed solely through use of one test image (Alderson liver and spleen, Alderson Research Laboratories, Stamford, CT), were applied to sets of 60 simulated images (ten noise realizations at each of six count levels) from three significantly different test images. Both the filter parameters and the NMSEs obtained were observed to not be significantly different from the count-dependent Metz filters designed specifically for these other test images.

MATERIALS AND METHODS

Object Images and Generation of Simulated Images

Four different 128 × 128 pixel, (technetium-99m (^{99m}Tc), images were used as "object" images in this study. These are shown in Figure 1. The first was an image of the Alderson liver and spleen phantoms filled with a ^{99m}Tc solution, and placed in contact with a super high resolution collimator on a large field of view SPECT camera (Dyna-Scan, Picker International, Highland Heights, OH). Over 200 million counts were collected to minimize noise in this "object" image. Similarly, images of an Iowa heart phantom (Cardiac Insert, Data Spectrum Corp., Chapel Hill, NC) (acquired at 1.5 magnification) and Alderson kidney phantoms were collected. The fourth "object" image was that of a posterior view of a patient undergoing bone imaging. It was collected with a super-high resolution collimator, a 15% energy window, and contained more than eight million counts.

Each of the "object" images had 60 simulated acquisition images generated from it in the following manner. First, the "object" image was blurred in the frequency domain by an MTF selected to simulate the "average" blurring which occurs during the acquisition of ^{99m}Tc SPECT images with our camera system (*13*). Next the blurred image was scaled to six different total count levels (25,000; 50,000; 100,000; 250,000; 500,000 and 1,000,000). Finally, ten Poisson noise realizations at each count level were generated from each of the scaled images (*13*).

The images of the Alderson liver and spleen phantoms were used to develop the CLS-Metz filter as detailed below. Then, the three other sets of images were used to test the adaptability of this filter to other objects. This was done by forming count-dependent Metz filters separately for each of these sets as described in the next section. Then, the filter parameters, and NMSEs obtained with these filters were compared to those obtained by applying the CLS-Metz filter designed using the Alderson liver and spleen images to these images.

Metz Filter

The linear restoration filter which was modified to be image-dependent was the Metz filter (*14*). The one-dimensional frequency domain form of the Metz filter is defined as:

$$M(f) = MTF(f)^{-1} \cdot [1-(1-MTF(f)^2)^X], \quad (1)$$

where f is the spatial frequency, MTF is the modulation transfer function, and X is a factor which controls the extent to which the inverse filter (first term on the right side of Eq. 1) is followed in the frequency domain before the low-pass portion of the filter (second term) dominates. In the present formulation of this filter, the MTF in the low-pass filter portion is replaced by a generalized exponential of the form

$$H(f) = \exp(-f^P/S), \quad (2)$$

where P is the exponent of the spatial frequency and S is a constant analogous to the variance of a Gaussian function (*8*, *14*,*15*).

Values for the parameters X, P, and S were obtained from optimization studies. These used the minimization of the NMSE between the liver and spleen "object" image and the simulated acquisition images generated from it as the opti-

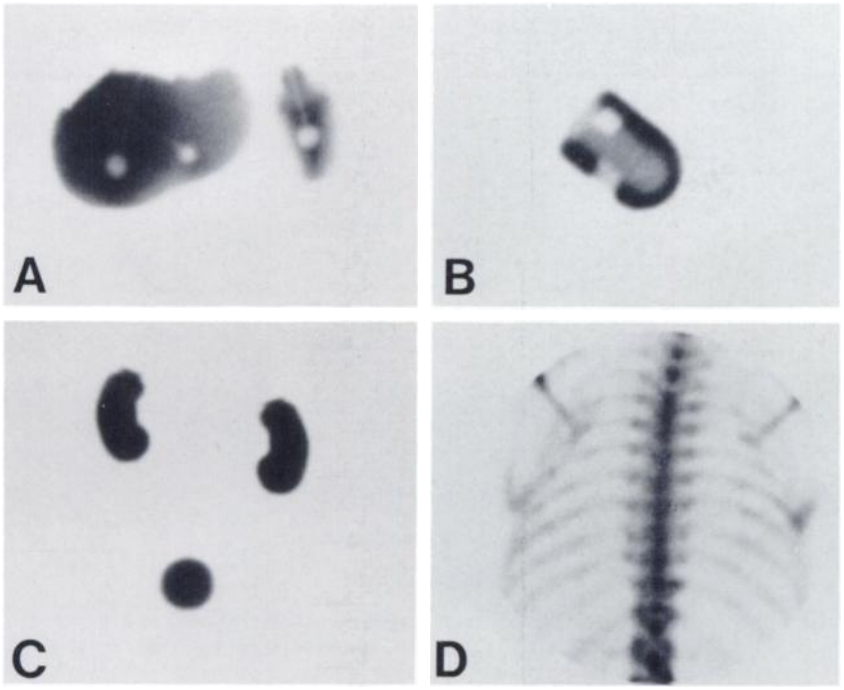

FIGURE 1
The four high count images used as "object" images in simulation studies. (A) Alderson liver and spleen, (B) Iowa heart phantom, (C) Alderson kidney phantoms and sphere to represent bladder, and (D) clinical posterior bone image.

mization criterion (*8,13,15*). Count-dependent Metz filters were formulated by determining P and S as fixed constants for a given MTF, and then linear regression was used to develop a functional relation between X and the total image count (*13*). In the past, S was also allowed to vary with count (*1,5*). However, the adoption of the use of the "true" MTF in the inverse filter portion of Eq. 1 eliminated the need for this added degree of complexity. This is demonstrated in Tables 1 and 2 where no significant difference in NMSEs was found between count-dependent Metz filters with S allowed to vary (row one) for the liver and spleen images, and when S was held fixed (row two). Holding S fixed reduced to one (X of Eq. 1) the number of variables which were needed to adapt for count level and object. Although not necessary for the formulation of the CLS-Metz filter, this simplification did facilitate the design task with virtually no loss in image quality as judged by the NMSE.

With S and P of Eq. 2 fixed to the values determined through use of the Alderson liver and spleen images, count-dependent Metz filters (values of X as a function of count) were determined in a similar manner for the other three sets of images. When the NMSEs resulting from this optimization process were compared to those determined for the same images when S, P, and X were allowed to vary, again no significant difference in the NMSE values was observed as shown in rows 1 and 2 of Tables 1 and 2. Thus, with the present formulation of the Metz filter (Eqs. 1 and 2), it is believed that S and P should be tailored to the MTF, and X to the individual images. The goal of the CLS-Metz filter was to automatically vary X for images significantly different from the Alderson liver and spleen images based upon parameters formulated using the Alderson liver and spleen images.

CLS-Metz Filter Formulation

In the frequency domain the constraint equation for the CLS filter is (*10,11*)

$$\sum \sum [G(f)\text{-}MTF(f)\cdot F(f)\cdot G(f)]^2 = n^2N, \qquad (3)$$

where G is the Fourier transform of the image, F is the restoration filter, n is the image dimension, and N is the average value of the noise power spectrum. This equation sets the sum of the squared residuals (the difference between the acquired image and the reblurred estimate of the true object) equal to the sum of the squared noise (*10–12*). With insertion of Eqs. 1 and 2 into Eq. 3, an estimate of N (*2,10*), and P and S of Eq. 2 determined for a given MTF, the only unknown is that of X. X can then be solved for in an iterative fashion (*10*) as that value which makes the two sides of Eq. 3 equal to within some tolerance (0.05% in the present implementation).

When the values of X resulting from use of Eq. 3 were compared with those which minimized the NMSE for the 60 simulated Alderson liver and spleen images, two problems were noted. First, there was an excessive amount of random variation in the values of X resulting from using Eq. 3 to determine X. The estimate of the noise power spectrum used in Eq. 3 when the scatter was noted was simply the total count (*10*). This has been shown to be a good estimate of the average value of the noise power spectrum (*2*). It does, however, have a certain amount of uncertainty associated with it. Another estimate of the noise power spectrum can be obtained by averaging the magnitudes of the image power spectrums at frequencies large enough for the contributions of the blurred object to be negligible. It was hypothesized that this average

TABLE 1
NMSEs* for ten 50,000 Count/Frame Simulated Images

Filter	Phantom			
	Liver and spleen	Iowa heart	Alderson kidneys	Posterior bone
"True" Minimum NMSE Metz***	0.0095	0.0080	0.0124	0.0357
	(0.0004)	(0.0006)	(0.0007)	(0.0014)
Constant S Minimum NMSE Metz****	0.0095	0.0081	0.0125	0.0361
	(0.0004)	(0.0007)	(0.0007)	(0.0014)
Count-Dependent Metz	0.0096	0.0148**	0.0191**	0.0362
	(0.0004)	(0.0007)	(0.0004)	(0.0015)
CLS-Metz	0.0096	0.0084	0.0127	0.0364
	(0.0004)	(0.0007)	(0.0007)	(0.0015)
Wiener	0.0148**	0.0114**	0.0196**	0.0451**
	(0.0029)	(0.0017)	(0.0015)	(0.0017)
CLS	0.0131**	0.0108**	0.0168**	0.0393**
	(0.0037)	(0.0022)	(0.0023)	(0.0024)
Count-Dependent Butterworth	0.0200**	0.0347**	0.0389**	0.0463**
	(0.0006)	(0.0012)	0.0007)	(0.0011)

* Average (SD) for ten simulated images of each phantom.

** Significant difference ($p > 0.05$) from true minimum NMSE value with S of Eq. 2 allowed to vary.

*** Value obtained from optimization of filter for the individual images of each object image set (i.e., liver and spleen, Iowa heart, Alderson kidneys, and bone, separately) with both X and S of Eqs. 1 and 2 allowed to vary.

**** Value obtained from optimization of filter for the individual images of each object image set (i.e., liver and spleen, Iowa heart, Alderson kidneys, and bone, separately) with X of Eq. 1 allowed to vary and S of Eq. 2 fixed at the value obtained with the liver and spleen images.

TABLE 2
NMSEs* for ten 500,000 Count/Frame Simulated Images

Filter	Phantom			
	Liver and spleen	Iowa heart	Alderson kidneys	Posterior bone
"True" Minimum NMSE Metz***	0.0037	0.0025	0.0050	0.0151
	(0.0001)	(0.0001)	(0.0003)	(0.0003)
Constant S Minimum NMSE Metz****	0.0037	0.0026	0.0050	0.0152
	(0.0001)	(0.0002)	(0.0003)	(0.0003)
Count-Dependent Metz	0.0037	0.0034**	0.0073**	0.0160
	(0.0001)	(0.0001)	(0.0003)	(0.0003)
CLS-Metz	0.0038	0.0027	0.0051	0.0152
	(0.0001)	(0.0002)	(0.0003)	(0.0003)
Wiener	0.0063**	0.0041**	0.0063**	0.0286**
	(0.0009)	(0.0014)	(0.0010)	(0.0025)
CLS	0.0045**	0.0029**	0.0061**	0.0190**
	(0.0037)	(0.0004)	(0.0004)	(0.0011)
Count-Dependent Butterworth	0.0169**	0.0302**	0.0341**	0.0362**
	(0.0002)	(0.0002)	(0.0003)	(0.0004)

* Average (SD) for ten simulated images of each phantom.
** Significant difference ($p < 0.05$) from "true" minimum NMSE value with S of Eq. 2 allowed to vary.
*** Value obtained from optimization of filter for the individual images of each object image set (i.e., liver and spleen, Iowa heart, Alderson kidneys, and bone, separately) with both X and S of Eqs. 1 and 2 allowed to vary.
**** Value obtained from optimization of filter for the individual images of each image set (i.e., liver and spleen, Iowa heart, Alderson kidneys, and bone, separately, with X of Eq. 1 allowed to vary and S of Eq. 2 fixed at the value obtained with the liver and spleen images.

value may provide a better estimate of the noise power for use in Eq. 3.

The second problem noted was that the values of X determined using the CLS method were consistently lower than those obtained using the minimization of the NMSE as the criterion. This is not too surprising since they are two different filter design criteria, and thus would probably produce different results. What was surprising, however, was that a regression equation could be used to closely predict the latter from the former. Nonlinear regression using the Gauss-Newton method (*16*) was used to fit the 60 values of X determined using the minimization of the NMSE as the criterion (X_{NMSE}) to the 60 values of X determined using the CLS constraint relation (X_{CL}), to the following form

$$X_{NMSE} = A \cdot X_{CLS}^{B} + C. \quad (4)$$

Here A, B, and C are the constants determined from the regression analysis.

For a given MTF, it was hypothesized that the regression equation developed for the simulated images of the Alderson liver and spleen could be used to obtain estimated values of X_{NMSE} from X_{CLS} for any other object. The test of this hypothesis is detailed in the section describing the test of the adaptability of the CLS-Metz filter.

Implementation of the CLS-Metz Filter

For a given MTF, once the parameters of the count-dependent Metz filter and the above regression relation have been defined using the simulated images of the Alderson liver and spleen phantoms, the CLS-Metz filter is implemented in the following manner for use with planar images. First, the image is windowed (multiplied by an array of values which decrease toward the edge) by a circularly symmetric function (*17*). The window used was symmetric about the center of the image with the central portion of the window equal to 1.0. The sides of the window rolled off from a value of 1.0 to a value of 0.0 by following a raised cosine function for the outer 10% of the diameter of the function (*17*). The window was used to minimize the influence of truncation of the object by the camera field of view on the image power spectrum. Without the windowing, the filter was observed, on occasion, to adapt to recovering edges at the sides of the camera field of view at the expense of image quality in the center.

Next, the Fourier transform of the image (G) is determined and an estimate of the average value of the noise power spectrum is obtained from the image power spectrum (G^2) to allow calculation of the right hand side of Eq. 3. For 128 × 128-images, this is estimated as the two-dimensional average of all frequency terms over one-half the Nyquist frequency. For 64 × 64-images, the two-dimensional average of all frequencies above seven-eighths of the Nyquist frequency is used.

The count-dependent Metz filter as optimized from the Alderson liver and spleen images is then used to provide an initial value for the value of X. This initial value is substituted into the following expression, which is the left-hand side of Eq. 3 after some algebraic manipulation using Eqs. 1 and 2:

$$\sum \sum [G(f) \cdot (1-H(f)^2)^X]^2. \quad (5)$$

The value of Eq. 5 is the frequency domain equivalent of the sum of the square of the residuals or the total "difference energy" (*10*). Notice that the term raised to the power X is just a high-pass filter since H of Eq. 2 is a low-pass filter. If the value of Eq. 5 is less than the total noise energy (right-hand side of Eq. 3), then X is increased by a factor of two (more deconvolution is performed). Evaluation of the differ-

ence energy is then conducted with this new value of X and the process repeated until the difference energy is less than the total noise energy. At this point, a Newton-Raphson iterative scheme (*10*) is used to obtain a final value of X which brings the agreement of the two sides of Eq. 3 to within 0.05%. If the initial value of X yielded a difference energy less than the total noise energy, X is decreased, rather than increased, by factors of two. This scheme prevents wild oscillations in successive values of X. The processing time to carry out such calculations varied with the number of iterations necessary to obtain agreement between the two sides of Eq. 3. On the average it took 4 sec for a 128 × 128-image and <2 sec for a 64 × 64-image when implemented on an array processor (AP400, Analogic Corp., Wakefield, MA).

The method used for determining CLS-Metz filters for SPECT images was slightly different because the SPECT acquisition set provides multiple, low-count, views of the same object. For SPECT images the value of X_{CLS} was determined for each image and then the average of these values was used to calculate a single value of X_{NMSE} and hence a single filter to be applied to the entire acquisition image set. An alternative method of Wiener low-pass filtering the individual values of X_{CLS}, and then using the filtered values of X_{CLS} to determine a different value of X_{NMSE} for each image has also been investigated for the CLS filter and could be used with the CLS-Metz filter (*11*). However, that method would have the drawback of allowing the filtering to produce an anisotropic point spread function.

Test of the CLS-Metz Filter's Adaptability

Since the parameters of the CLS-Metz filter, (P, S, and regression terms of Eq. 4) were developed solely through use of the simulated images from the Alderson liver and spleen phantoms, it was essential to test the adaptability of this filter to other objects before any claim of reasonable image-dependence can be made. This testing was performed in two parts. In the first the predicted values of X_{NMSE} obtained from the CLS-Metz filter were compared using linear regression (*18*) to the values of X obtained when the Metz filter was individually optimized using the minimization of the NMSE as the criterion for each of the 60 simulated images of the three test phantoms. Since the probability distribution for these values of X was unknown, the nonparametric sign test (*18*) was used to compare the predicted and actual minimum NMSE values of X for a statistically significant difference.

The second test of adaptability was to compare the NMSE values (an index of overall image fidelity) obtained when using the CLS-Metz predicted and actual minimum NMSE determined values of X to form filters. Calculation of the NMSE also allowed comparison of the CLS-Metz filter to other image-dependent restoration filters. The filters selected for this comparison were the Wiener (*2*), and the CLS (*10*) filter. It should be noted that neither of these filters required simulated images to optimize their parameters. Comparison to a count-dependent Butterworth low-pass filter (*10*) also was performed to determine the extra gain in image quality provided by use of restoration filters. This filter was designed using the Alderson liver and spleen images. The statistical significance of the variation in NMSEs between filters was determined using one-way analysis of variance (*18*). When a significant difference was observed between the means of the various filters at a p value of 0.05 or less, Sheffe's method of comparing paired means for a significant difference was used to compare each to the "true" minimum NMSE values.

RESULTS

Figure 2 shows count-dependent Metz filters derived for each of the four test image sets of the objects of Figure 1. In each of the plots, the system MTF (bottom curve), the inverse filter (top curve), and six Metz filters for the counts used in creating the simulated image sets (25,000; 50,000; 100,000; 250,000; 500,000; and 1,000,000 counts) are plotted. Spatial frequency is re-

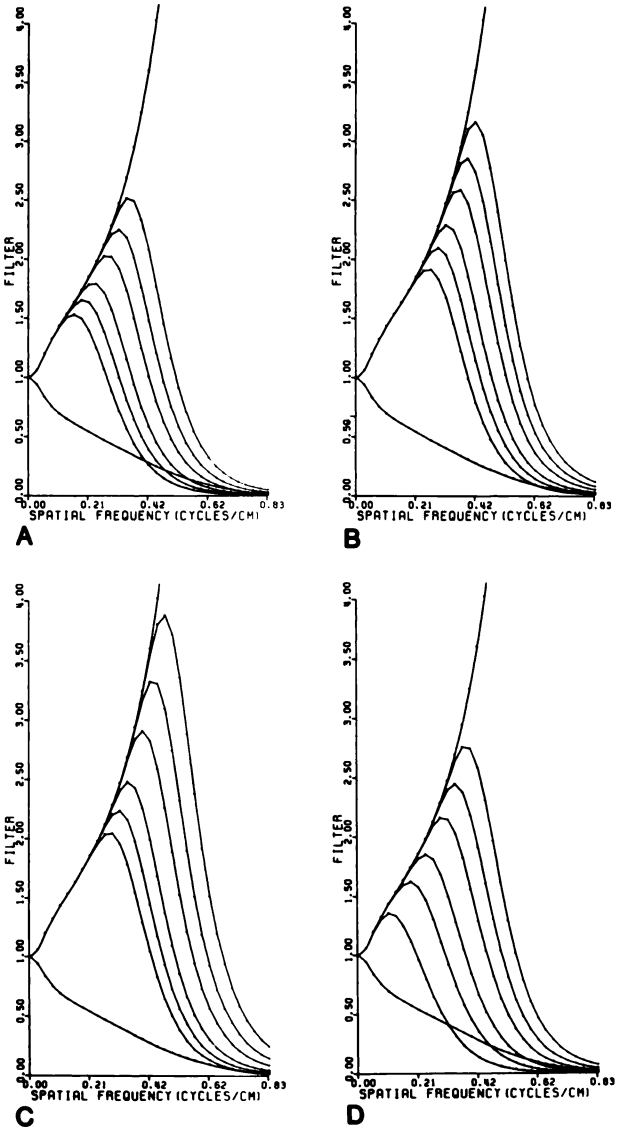

FIGURE 2
Plots of a ^{99m}Tc system MTF (lowest curve), inverse filter (highest curve), and six Metz filters for total counts of 25,000; 50,000; 100,000; 250,000; 500,000; and 1,000,000 (the six curves in between) for (A) Alderson liver and spleen phantom; (B) Iowa heart phantom; (C) Anderson kidney phantoms; and (D) posterior clinical bone image.

ported as cycles/cm in the plots. The end-point frequency in each is equivalent to 0.25 cycles/pixel for a 128 × 128-pixel acquisition or 0.5 cycles/pixel for a 64 × 64-pixel acquisition. Notice the large variation between the filters at a given count level and variation with count for a given object. This verifies the need for both count- and object-dependence in filter formulation.

Figure 3 illustrates the steps in the development of the CLS-Metz filter. Figure 3A shows a plot of the 60 values of X determined to minimize the NMSE in each of the simulated images of the Alderson liver and spleen phantoms vs. the values of X determined from the CLS-Metz filter using the total image count as an estimate of the noise power spectrum and no use of the regression relation of Eq. 4. The line in this figure, and all subsequent figures, is the line of identity to be used for comparison purposes. Notice the large amount of scatter in the values and the trend of the predicted value of X to be lower than the actual value of X which minimized the NMSE. Table 3 gives the results of the linear regression and Sign test comparison of the predicted and actual values of X. A low slope, poor correlation coefficient, and significant difference by the Sign test were obtained with this formulation. Use of the average of the high frequency values of the image power spectrum as an estimate of the noise power spectrum was observed to decrease the scatter in the values of X as shown in Figure 3B, and by the improved correlation coefficient of Table 3. However, there is still a significant bias between the two sets of values. The regression relation of Eq. 4 is seen to be able to remove this bias as illustrated in Figure 3C and by the slope of nearly 1.0 and lack of a significant difference by the Sign test as reported in Table 3. Thus, the final formulation of the CLS-Metz filter is seen to be able to perform as well as the count-dependent Metz filter for the images used to develop it. It is when it is applied to other images that the advantage of the CLS-Metz's image dependent formulation manifests itself.

Figure 4 and Table 3 summarize the results of the first part of the test of the adaptability of the CLS-Metz filter. From Table 3 it can be seen that the count-dependent Metz filter formed for the Alderson liver and spleen images performs poorly when applied to the 180 test images (ten at each of six count levels for the three different starting objects of Figure 1B–D). The CLS-Metz filter without use of the regression relation of Eq.

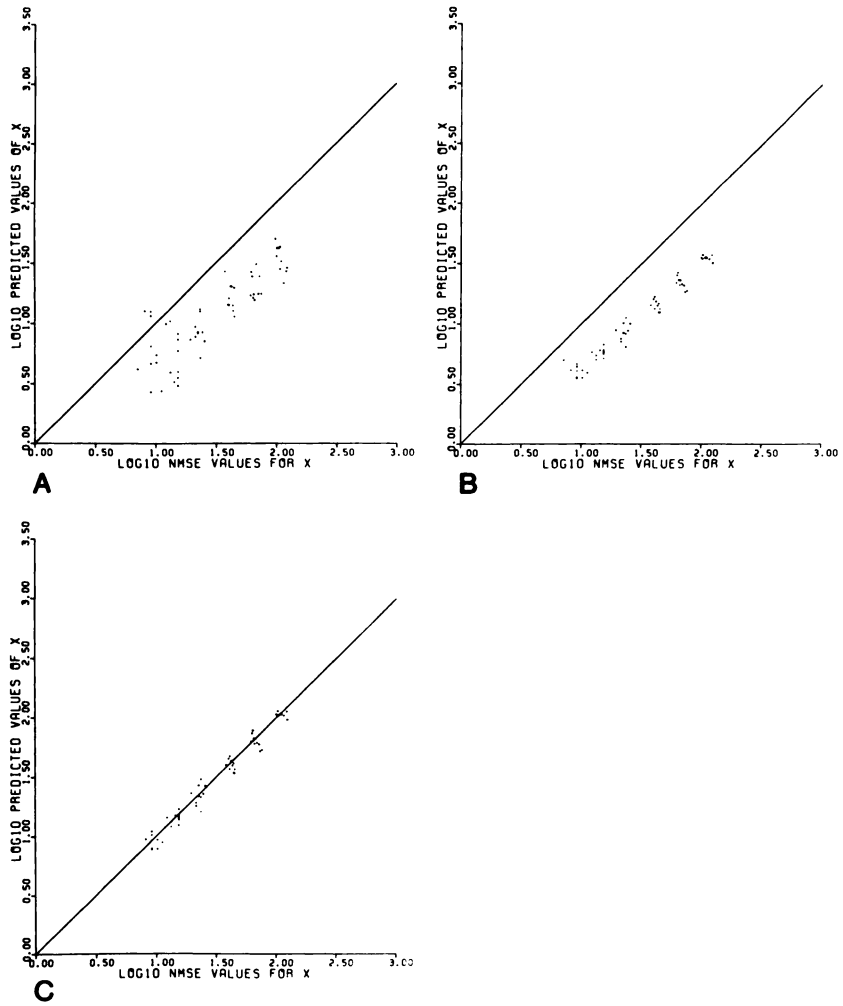

FIGURE 3
Plot of the logarithm of the values of X of Eq. 1 resulting from the resolution of Eq. 3 vs. the logarithm of the values of X determined by minimizing the NMSE for the 60 simulated images of the Alderson liver and spleen phantom. The diagonal line in each case is the line of identity not the regression line. (A) Estimate of noise power equal to the total image count. (B) Estimate of noise power equal to the average of the high frequency portion of the image power spectrum and (C) estimate of the noise power equal to the average of the high frequency portion of the image power spectrum and use of the regression relation.

TABLE 3
Linear Regression Relations Between Predicted Values of X and Values of X Determined to Minimize the NMSE

Phantom	Filter	Slope	Intercept	Correlation coefficient	Sign test
Liver Spleen†	Count*	0.99	0.5	0.99	NS
	CLS-Metz**	0.34	0.3	0.93	<0.05
	CLS-Metz***	0.36	0.1	0.99	<0.05
	CLS-Metz****	0.98	0.1	0.99	NS
Three test objects	Count*	0.21	14.8	0.81	<0.05
	CLS-Metz***	0.29	0.1	0.97	<0.05
	CLS-Metz****	0.95	0.1	0.98	NS

* Count-dependent Metz filter optimized for Alderson liver and spleen images.
** CLS-Metz filter optimized for Alderson liver and spleen images with the noise power estimated as the total image count and no use of regression relation of Eq. 4.
*** CLS-Metz filter optimized for Alderson liver and spleen images with the noise power estimated as the average of the high frequency components and no use of the regression relation of Eq. 4.
**** CLS-Metz filter optimized for Alderson liver and spleen images with the noise power estimated as the average of the high frequency components and with use of the regression relation of Eq. 4 developed for the Alderson liver and spleen images.

4 developed for the liver and spleen phantoms is seen to perform a little better. In particular, it has a better correlation coefficient. The good correlation coupled with the results of the plot of Figure 4A indicate that a single regression relation would likely work for all three sets of test images. In Figure 4B and Table 3, it can be seen that the regression relation developed for the Alderson liver and spleen phantoms works quite well for these other test images. Notice the slope near 1.0, the good correlation coefficient, and the lack of a significant difference by the Sign test. This is true even though the values of X for these phantoms covered a considerably larger range than those of the Alderson liver and spleen images. Thus, it appears that the CLS-Metz filter can be developed for one set of clinically reasonable simulated images and be able to adapt, in a near-optimal

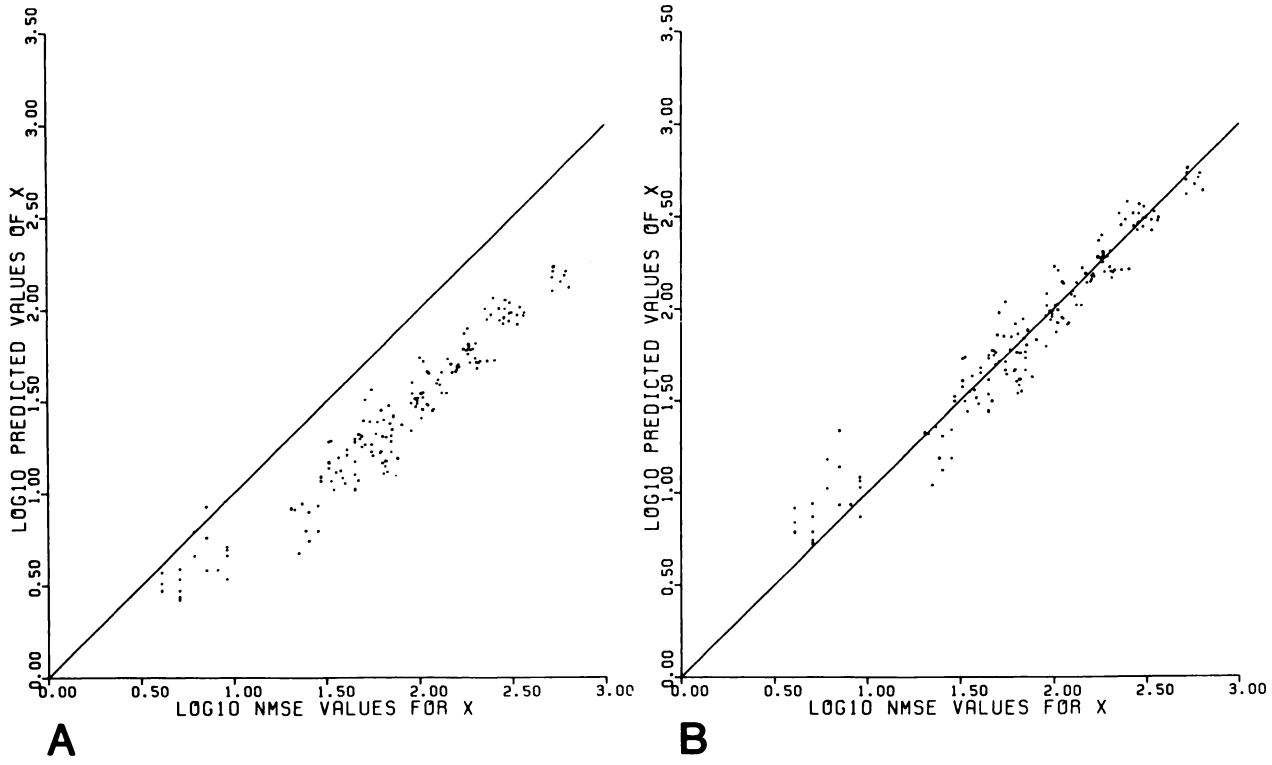

FIGURE 4
Plot of the logarithm of the values of X of Eq. 1 resulting from the solution of Eq. 3 vs. the logarithm of the values of X resulting from minimizing the NMSE for 60 images of each of the three test images. The diagonal line in each case is the line of identity not the regression line. (A) No use of regression relation and (B) use of regression relation.

fashion, to images from other test objects. This conclusion has been verified for other MTFs. However, it should be noted that for each MTF a new set of parameters needs to be determined.

The second test of adaptability was that of comparing the NMSE values obtained with the use of various filters to the "true" minimum values obtained when the Metz filter was optimized for each image. The results of this comparison for the 50,000 count level images are shown in Table 1, and for the 500,000 count level images in Table 2. In these it can be noted that the CLS-Metz filter never results in an NMSE significantly different from the true minimum values; whereas, the liver and spleen optimized count-dependent Metz, the Wiener, and CLS filters do. It also should be noted that the restoration filters in all cases perform significantly better than two-dimensional low-pass filtering. Comparison of the NMSE values of Tables 1 and 2 shows that as the count increases from 50,000 to 500,000 counts/frame, the restoration filters are able to produce more of an improvement in image fidelity than the low-pass filter. This is because as the count increases, the restoration filters are able to deconvolve the image to a greater extent in the frequency domain (*1*).

The data in Table 3 indicate that the image-dependent Metz filter can more accurately predict the optimal value of X in Eq. 1 than the count-dependent Metz filter can for objects other than the liver-spleen phantom. The difference in image quality when these filters are applied to clinical images is illustrated in Figures 5 and 6. In these figures, all three of the two-dimensional filters were designed using solely the Alderson liver and spleen images. The image quality improvement due to the CLS-Metz filter, which is seen in this example, also has been consistently noted in clinical studies.

DISCUSSION

This study reports the development and testing of an image-dependent, restoration filter. A linear filter was studied because its relatively fast execution time makes it attractive for use with the array processors presently at clinical sites. Nonlinear, statistically based restoration techniques may ultimately provide better image quality (*19*); however, their increased computational burden makes them too time consuming for extensive clinical use at present.

In terms of the NMSE, the CLS-Metz filter was shown to provide significantly better image fidelity than two other image-dependent filters to which it was compared (Tables 1 and 2). The CLS filter (*10*) performed better than the Wiener (*2*) and the count-dependent Metz filter for the Iowa Heart and Alderson kidney phantoms. In terms of the NMSE, it never performed as well as the CLS-Metz filter, however. This may be an unfair comparison, though, because the minimization of the NMSE is not the criterion of the CLS filter (*10*). In a test of image preference (*10*), the CLS filter was observed to perform better than the Metz. Also, it

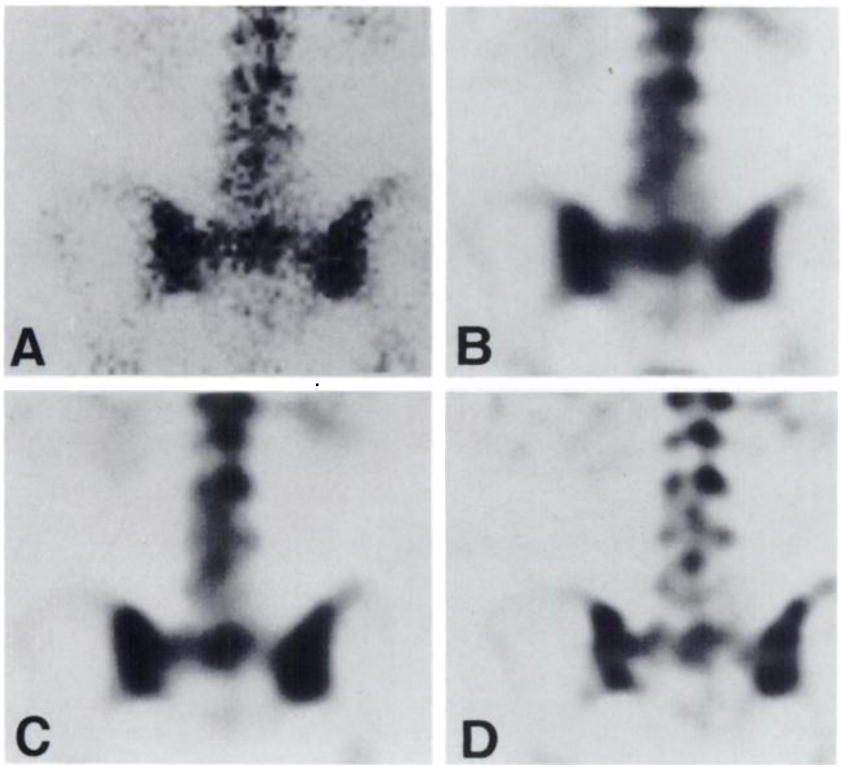

FIGURE 5
Comparison of different methods of filtering a posterior view from planar acquisition SPECT image set of a 180° clinical bone study. (A) Raw data; (B) Two-dimensional Butterworth smoothing; (C) Count-dependent Metz restoration; and (D) Image-dependent Metz restoration.

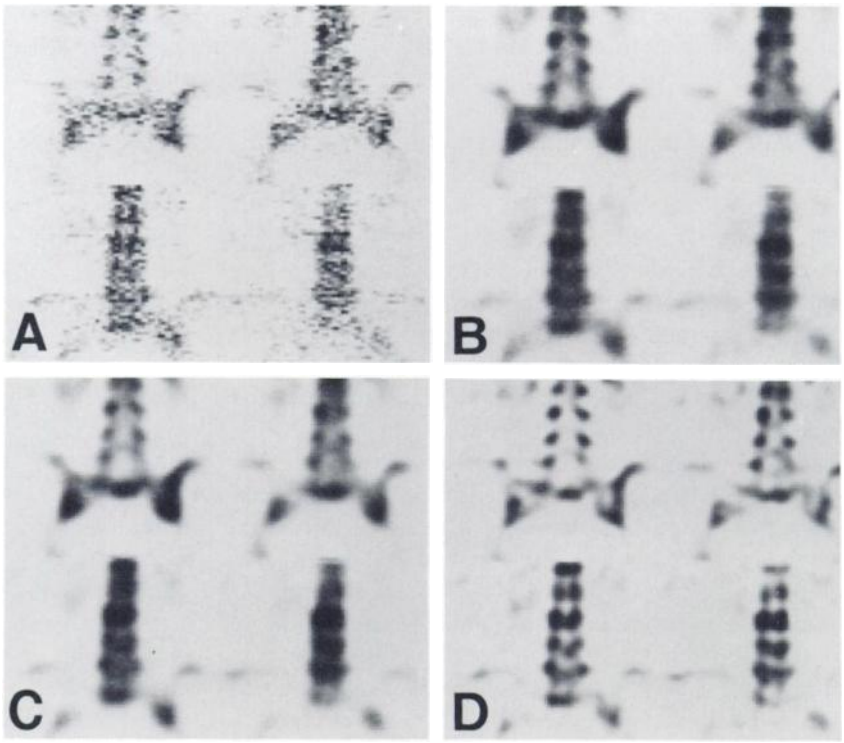

FIGURE 6
Comparison of four selected coronal slices from the bone study of Figure 3. Images were reconstructed by "ramp" filtering the projection data after two-dimensional filtering of acquisition images by: (A) no prefiltering; (B) Butterworth smoothing; (C) count-dependent Metz restoration; and (D) image-dependent Metz restoration.

is easier to implement because it does not require the use of parameters obtained from optimization studies with simulated images. At present, an ROC study is being planned to help differentiate between these filters on the basis of observer performance.

The use of the average of the magnitudes of the image power spectrum at frequencies large enough for the contribution of the blurred object to be negligible was determined to be better than using the total count as the estimate of the noise power spectrum as seen in Figure 3 and Table 3. By Eq. 5, the difference energy is calculated as the sum of the squared magnitudes of the product of the Fourier transform of the image and a high-pass filter. At frequencies where the high-pass filter is essentially 1.0, this becomes the sum of the image power spectrum. Thus use of the average of the high frequency terms as the estimate of the noise power spectrum provide a matching of the values obtained from each side of Eq. 3 at these frequencies. This is one way of explaining the poorer results (Fig. 3 and Table 3) seen with use of the total count as the estimate of the noise power spectrum.

CONCLUSIONS

Image-dependent restoration filters are required to provide an optimal compromise between noise suppression and image deconvolution (removal of blurring). An image-dependent Metz filter has been formulated which adapts to different test "object" images to provide near optimal image fidelity in the NMSE sense. It also has been shown to provide consistently good image quality with clinical images as diverse as liver and spleen studies and bone studies.

ACKNOWLEDGMENTS

The authors thank Dr. Paul Doherty and Mr. Ronald Schwinger for their continued advice and encouragement, and Dr. Monroe Jahns for suggesting use of high count clinical images. This investigation was aided by a grant from Centocor Corporation, and grant number CA42165 from the National Cancer Institute.

REFERENCES

1. King MA, Doherty PW, Schwinger RB, et al. Fast-count dependent digital filtering of nuclear medicine images. *J Nucl Med* 1983; 24:1039–1045.
2. King MA, Doherty PW, Schwinger RB, et al. A Wiener filter for nuclear medicine images. *Med Phys* 1983; 10:876–880.
3. Miller TR, Goldman KJ, Epstein DM, et al. Improved interpretation of gated cardiac images by use of digital filters. *Radiology* 1984; 152:795–800.
4. Maeda J, Murata K. Digital restoration of scintigraphic images by a two-step procedure. *IEEE Trans Med Imag* 1987; 6:320–324.
5. King MA, Schwinger RB, Doherty PW, et al. Two-dimensional filtering of SPECT images using the Metz and Wiener filters. *J Nucl Med* 1984; 25:1234–1240.
6. Webb S, Long AP, Ott RJ, et al. Constrained deconvolution of SPECT liver tomograms by direct digital

image restoration. *Med Phys* 1985; 12:53–58.
7. Madsen MT, Park CH. Enhancement of SPECT images by Fourier filtering the projection image set. *J Nucl Med* 1985; 26:395–402.
8. King MA, Schwinger RB, Penney BC, et al. Digital restoration of In-111 and I-123 SPECT images with optimized Metz filters. *J Nucl Med* 1986; 27:1327–1336.
9. Yanch JC, Flower MA, Webb S. A comparison of deconvolution and windowed subtraction techniques for scatter compensation in SPECT. *IEEE Trans Med Imag* 1988; 7:13–20.
10. Penney BC, King MA, Schwinger RB, et al. Constrained least squares restoration of nuclear images: selecting the coarseness function. *Med Phys* 1987; 14:849–858.
11. Penney BC, King MA, Schwinger RB, et al. Modifying constrained least squares restoration for application to SPECT projection images. *Med Phys*, 1988; 15:334–342.
12. Trussell HJ. Convergence criteria for iterative restoration methods. *IEEE Trans Acoust, Speech, Signal Process* 1983; 31:129–136.
13. King MA, Schwinger RB, Penney BC. Variation of the count-dependent Metz filter with imaging system modulation transfer function. *Med Phys* 1986; 13:139–149.
14. Metz CE, Beck RN. Quantitative effects of stationary linear image processing on noise and resolution of structure in radionuclide images. *J Nucl Med* 1974; 15:164–170.
15. King MA, Glick SJ, Penney BC, et al. Interactive visual optimization of SPECT pre-reconstruction filtering. *J Nucl Med* 1987; 28:1192–1198.
16. Neter J, Wasserman W, Katner MH. *Applied linear regression models*. Homewood, IL: Richard D. Irwin, Inc.; 1983:472–479.
17. Hamming RW. Digital filters. Englewood Cliffs, NJ: Prentice-Hall; 1977:178–179.
18. Pollard SH. A handbook of numerical and statistical techniques. New York: Cambridge University Press; 1977:167–179; 256–274.
19. Andrews HC, Hunt BR. Digital image restoration. Englewood Cliffs, NJ: Prentice-Hall; 1977:187–208.